Metastable magnetic domain walls in cylindrical nanowires

C.A. Ferguson, D.A. MacLaren, S. McVitie *

SUPA, School of Physics & Astronomy, The University of Glasgow, Glasgow G12 8QQ, United Kingdom

ABSTRACT

The stability of the asymmetric domain wall (ATDW) in soft magnetic cylindrical nanowires and nanotubes is investigated using micromagnetic simulations. Our calculated phase diagram shows that for cylindrical permalloy nanowires, the transverse domain wall (TDW) is the ground state for radii below 20 nm whilst the Bloch point wall (BPW) is favoured in thicker wires. The ATDW stabilises only as a metastable state but with energy close to that of the BPW. Characterisation of the DW spin structures reveals that the ATDW has a vortex-like surface spin state, in contrast to the divergent surface spins of the TDW. This results in lowering of surface charge above the critical radius. For both cylindrical nanotubes and nanowires we find that ATDWs only appear to exist as metastable static states and are particularly suppressed in nanotubes due to an increase in magnetostatic energy.

© 2015 The Authors. Published by Elsevier B.V. This is an open access article under the CC BY license (http://creativecommons.org/licenses/by/4.0/).

1. Introduction

Much research into domain walls (DWs) in magnetic nanowires has focused on flat, planar DW guides that have potential spintronic applications including racetrack memory [1], shift registers [2] and domain wall logic devices [3]. In these two dimensional (2-D) systems, and in the absence of strong magnetocrystalline anisotropy, the magnetisation is restricted to lie in-plane, pointing along the wire axis to form head-to-head or tail-to-tail Néel DWs. The spin microstructure of the DW itself then depends on the nanowire dimensions, as summarised by phase diagrams [4, 5] that in the case of soft magnetic materials such as permalloy (Py) identify three principal DW types. For wide, thick wires, the high magnetostatic energy associated with an abrupt head-to-head wall can be reduced by the inclusion of a vortex state. However, there is a minimum vortex diameter set by exchange energy so that reduction of the wire width below this value leads to a first-order [5] phase change and the production of a transverse DW. This second DW type has a triangular region of magnetisation lying perpendicular to the wire axis and its formation can be mediated by the third DW type, an asymmetric transverse DW, which has both a triangular form and retains some of the curling magnetisation of the vortex state but lacks a vortex core. Both the DW structure and its chirality are important for applications since they have been shown to influence the DW pinning potential [6]. In addition, a number of studies have shown the importance of metastable states, particularly in dynamic systems, where the DW

is shifted using a spin-polarised current or applied magnetic field. Experiments have shown that DWs can change type during propagation along the guide. Indeed, propagation of DWs in planar nanowires is ultimately limited by Walker breakdown, [7] which describes a process whereby an anti-vortex structure is periodically nucleated and annihilated at the wire edges [8], causing the motion of the DW to become non-uniform. A full understanding of both ground state and metastable (or transient) DW structures is therefore essential for device design.

In contrast to planar guides, the three dimensional (3-D) nature of cylindrical nanowires (CNWs) and cylindrical nanotubes (CNTs) has attracted interest because simulations and numerical models have predicted it to suppress Walker breakdown [9,10] in favourable cases. These 3-D structures lack lateral edges, thus preventing the nucleation of individual anti-vortex states and leading to the prediction that Walker breakdown by the nucleation of a single anti-vortex is topologically forbidden [11]. In other respects, many phenomena of 2-D nanowires have analogues in the 3-D case. Studies of magnetisation reversal in soft magnetic CNWs reveal that two distinct DWs are stable [12,13] – a transverse domain wall (TDW) and a Bloch point wall (BPW) and are related to the 2-D transverse and vortex states, respectively. The situation is similar for CNTs, except that a Bloch point need not form in the absence of a magnetic core along the CNT axis, producing instead a vortex DW (VDW) that has a similar external spin structure to the BPW [12]. Phase diagrams again show that the TDW is the ground state for thinner wires; the BPW/VDW for thicker wires. One might therefore expect the analogy with 2-D structures to continue and so predict the existence of a third DW structure; and a recent electron holography study [14] identified the existence of a such a

* Corresponding author.
E-mail address: Stephen.McVitie@glasgow.ac.uk (S. McVitie).

structure, an asymmetric transverse domain wall (ATDW). This observation opens up the little-explored possibility of metastable states in CNWs and CNTs. Here, we use micromagnetic simulations to study the 3-D ATDW in more detail. We simulate all three DW types across a range of cylinder and tube dimensions to map their stability and derive a phase diagram. The internal and surface spin structure of each DW is characterised, then used to inform a discussion of the ease of identifying each DW experimentally.

2. Methods

Simulations of CNWs and CNTs were performed using the Nmag [15] finite element package due to its suitability to simulating curved structures, and checked against results from the object oriented micromagnetic framework [16] (OOMMF) package. The range of radii simulated was 5–50 nm and the length was fixed at 2 μm, sufficient to ensure that domain reversal occurs via DW propagation [12]. Material parameters typical of permalloy were used: magnetisation, $M_s = 8.6 \times 10^5$ A m^{-1}; exchange constant, $A = 1.3 \times 10^{-11}$ J m^{-1}; anisotropy constants, $K_1 = K_2 = 0$. Following an approach adopted previously [6,17], the damping parameter was set to $\alpha = 0.5$, which is artificially high but allows the simulation to relax quickly without otherwise compromising results. It is expected that phase diagrams for soft magnetic materials scale with the exchange length [18,19], so the results will be important for all systems where the energetic contribution of magnetocrystalline anisotropy is insignificant. The maximum node spacing for all Nmag simulations was 5 nm and the voxel size in OOMMF was $5 \times 5 \times 5$ nm^3, both of which were scaled to be less than the exchange length of 5.3 nm. Preliminary simulations showed that only three DW types could be stabilised, i.e. the TDW, BPW and ATDW. An important aspect of these simulations was to assess the metastability of walls, independent of the magnetic ground state. To achieve this, each of the three preliminary DW types was expanded/contracted and interpolated onto the required starting mesh, then allowed to relax to the local energetic minimum. Thus, we created a BPW, TDW or ATDW starting state for each radius in the range and determined whether or not it would stabilise.

3. Results and discussion

3.1. Cylindrical nanowire results

Fig. 1 shows a 3-D view and cross-section of each of the three head-to-head DW configurations: (a) TDW, (b) ATDW and (c) BPW. The colours represent the axial component of magnetisation, M_z, while the arrows show the surface spin configuration. The thinnest wires support a TDW, illustrated in Fig. 1(a), in which the magnetisation meets and rotates to lie transverse to the wire axis, breaking the cylindrical symmetry. In contrast to the 2-D transverse DW, in which the transverse region has two degenerate orientations, the transverse component of the (3-D) TDW has no fixed direction and can point at any azimuthal angle. This rotational degeneracy is evident in simulations that show a corkscrew motion of the DW about the wire axis as it propagates under the torque of applied field or spin-polarised current [9,13]. Much thicker wires relax to the BPW structure of Fig. 1(c), in which the magnetisation in the DW wraps around the wire axis. A cross-section through the wire shows a vortex-like structure, at the centre of which is a micromagnetic singularity or Bloch point. As discussed below, the external spin structure of the BPW is similar to that of the VDW, which is observed in CNTs. Previous simulations show that the dynamic behaviour of VDWs under an applied
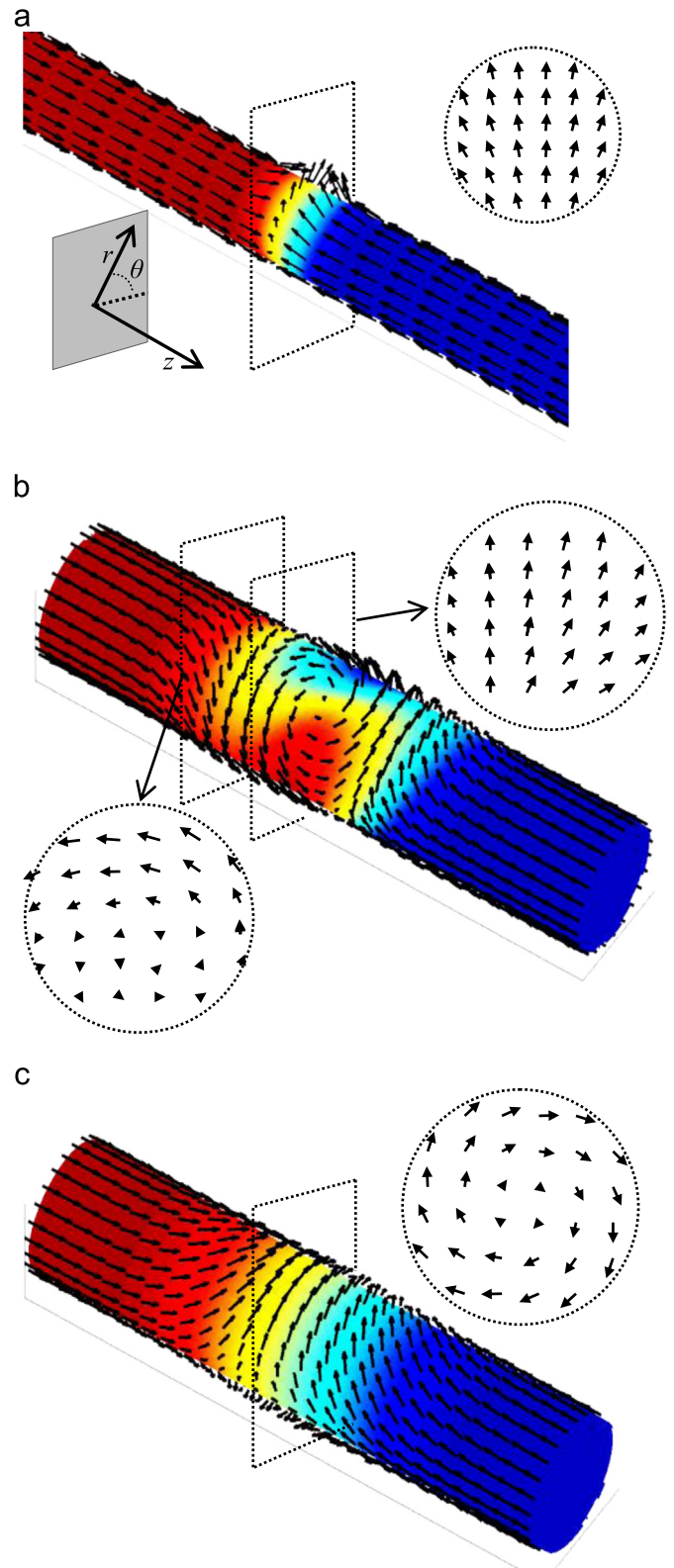
Fig. 1. The micromagnetic structure of (a) a transverse domain wall (TDW), (b) an asymmetric transverse domain wall (ATDW) and (c) a Bloch point domain wall (BPW) in soft ferromagnetic cylindrical nanowires. The external spin structure of the BPW is similar to that of the vortex domain wall (VDW) found in nanotubes. Colours indicate the magnitude of the axial component of magnetisation, M_z, in accordance with the arrows, which indicate the surface spin directions. The transition from red to blue therefore indicates the wall width. Cross-sections through the domain walls (in the r, θ plane), taken at the location of the wireframes, are inset.

field is dependent on the direction of the applied field and the resulting chiral interaction with the VDW vorticity [11,20]. The degeneracy of left- and right-handed configurations is broken in an applied axial field because of the chirality of the resulting torque on the DW's radial component of magnetisation, producing a DW distortion that depends on the sense of the field and the wall.

The third DW structure is illustrated in Fig. 1(b). By analogy with the 2-D case, it is referred to as an ATDW, although its spin configuration differs substantially from that of either the TDW or the BPW. Cross-sections through the wire on either side of the vortex/anti-vortex pair show the magnetisation to rotate about the wire axis, but unlike the BPW, the direction of rotation of the resulting axial vortices is of opposite sense on either side of the wall. The ATDW lacks both the axial rotational symmetry of the BPW and the mirror plane of the TDW, but has a clear vortex spin structure on its surface that we will show to be coupled to an anti-vortex structure underneath, rather similar to a transient structure predicted to exist in CNTs during DW propagation [11] and Walker breakdown. The range over which the ATDW is found to be metastable may therefore give an indication as to the CNW dimensions for which Walker breakdown would occur.

Fig. 2 summarises our results as a phase diagram that shows the magnetic energy density as a function of radius for the three stable DW configurations. The upper (full) lines indicate the variation of total magnetic energy whilst the lower (dot-dashed, dashed) lines show the variation of magnetostatic and exchange energy components (respectively). Note that we plot the energy *densities* in order to facilitate comparisons of wires of different diameters and to better display *relative* changes across the diagram. As the wires are of the same length, this normalisation gives a perspective on the localisation of exchange and magnetostatic energy terms along the length of the wire, which is useful since high energy densities are unfavourable. The phase diagram shows the ground state to be a TDW for wires of small radius and a BPW
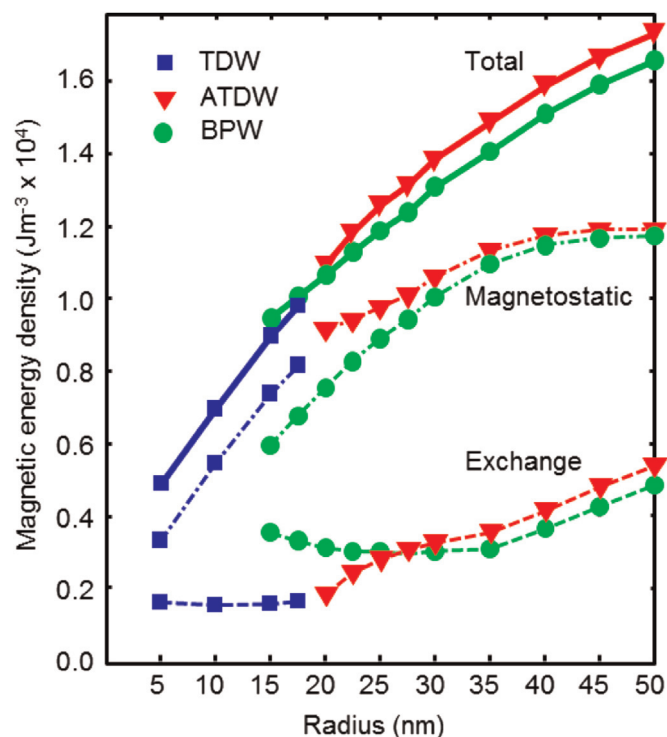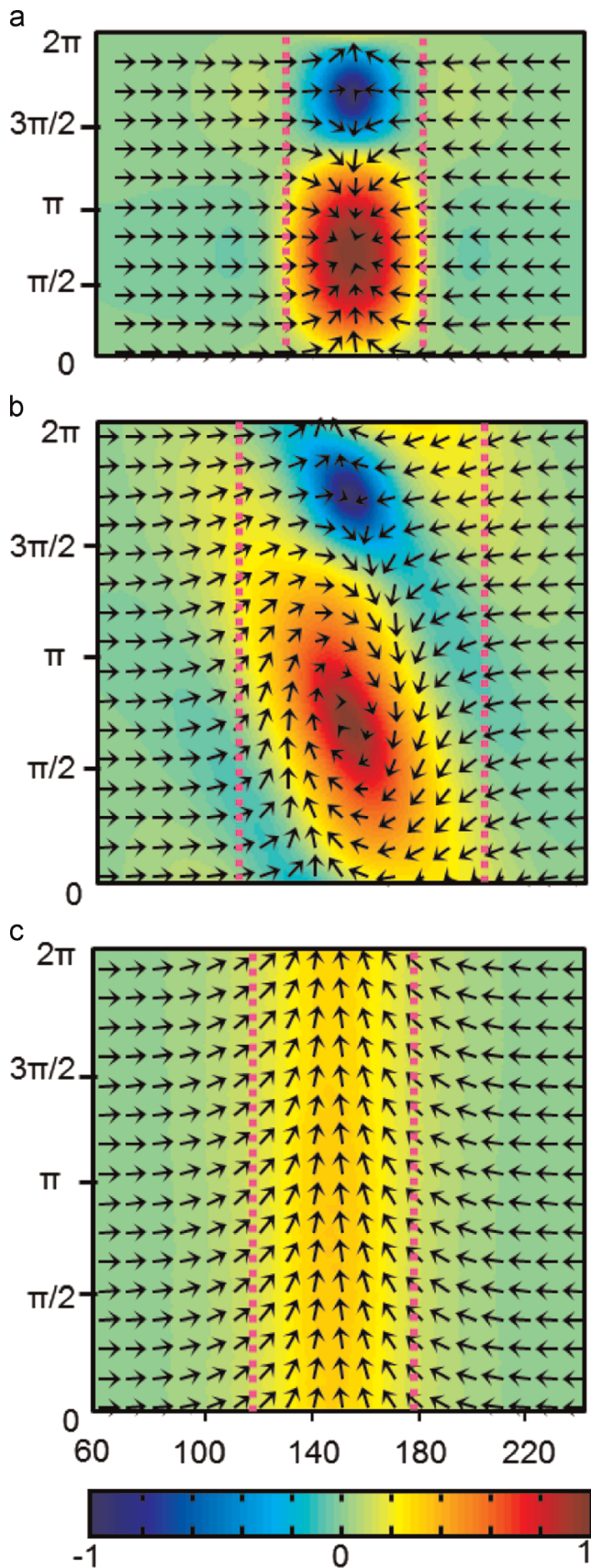
for thicker wires, with the phase change occurring at 20 nm for Py, in agreement with previous studies [13]. We can now also identify the ATDW as a metastable state spanning a similar range of geometries as the BPW, i.e. for radii greater than or equal to 20 nm in Py. The stability of the TDW at small radii and the BPW at larger radii is readily rationalised by consideration of the individual energy components and is similar to the 2-D case. Although the spins wrapping around the surface of the wire in the BPW minimise magnetostatic energy, the resulting axial vortex configuration has a minimum diameter set by exchange energy terms so that below a 20 nm radius, the exchange energy increases and the BPW structure becomes unfavourable. The TDW, on the other hand, has a much lower exchange energy contribution and is dominated by a substantial magnetostatic contribution arising from the surface magnetic poles implied by the cross-section of Fig. 1(a).

An interesting feature to note is the close proximity of the BPW and ATDW plots in Fig. 2, indicating that there is little difference in energy between the ground state BPW and the metastable ATDW. This is significant for experimental work and potential device applications since any imperfections in a wire could act as pinning sites and facilitate a change of DW between types of comparable energy; similarly, transient ATDWs should be expected in dynamic systems, but perhaps only above the 20 nm critical radius.

Another significant feature of the phase diagram is that the plots for the TDW and ATDW follow the same trend but do not share a stable structure at any dimension in this range, suggesting a greater similarity in spin structure than is apparent from Fig. 1. A more instructive view of the surface spin structure can be obtained by unrolling the outer layer of magnetisation, giving a two dimensional view. This "unrolled" surface magnetisation is shown in Fig. 3 for each DW and brings out the similarities between the TDW (Fig. 3(a)) and ATDW (Fig. 3(b)) structures. The figure uses a colour map to represent the out-of-plane component, M_r. Arrows display the direction of the surface in-plane components of magnetisation, M_z and the tangential component, M_θ. M_r provides a direct visualisation of the surface charge. In fact, our simulations show that volume charges are small compared to the surface charges for all DWs described in this paper (see below), which makes the unrolled view useful from an experimental point of view since the magnetic charge distribution provides the main contrast mechanism in magnetic force microscopy (MFM). From that perspective, the distribution of surface charges suggests that the BPW (Fig. 3(c)) would give rise to less contrast in MFM than could be expected from the other two wall types, given the large concentration of charge associated with their surface spin structures. Of course, DW observation using MFM depends on the relative orientation of the nanostructure on the substrate, which may cause some difficulty in DW identification as the localised charges of the TDW and ATDW may not align at a favourable azimuthal angle for strong MFM contrast. Lorentz electron microscopy and electron holography, on the other hand, could offer a better way of distinguishing the BPW from the other DW types since they are sensitive to the projected magnetisation and external field distribution as well as having the ability to change their viewpoint by simply tilting the sample about the long axis of the wire. The cylindrical symmetry of the BPW will appear distinct from the other DWs. Fig. 3 also indicates that the TDW is narrower than both the BPW and ATDW, offering a further means of discrimination. The vertical pink dashed lines in the figure indicate the effective wall width (calculated as elsewhere [21]); the indicated differences in wall length could be used to distinguish different DWs in both MFM and electron microscopy techniques.

The TDW offers perhaps the most striking surface spin structure, with two distinct features within the region of the wall. The blue area at the top of Fig. 3(a) is readily identified as an anti-vortex spin configuration; however, alongside it is a highly


Fig. 2. A micromagnetic phase diagram for head-to-head magnetic domain walls in cylindrical permalloy nanowires, showing the variation in total magnetic energy (full lines) and its main components (dashed lines) for transverse domain walls (TDWs), asymmetric transverse (ATDW) and Bloch point domain walls (BPWs).

Fig. 3. The 'unrolled' surface spin structures of typical (a) TDW, (b) ATDW and (c) BPW domain walls. Colours represent M_r, the radial component of magnetisation, in accordance with the colour bar key at the bottom. Lime green therefore represents magnetisation lying along the nanowire axis, z. Arrows show the direction of in-plane surface magnetisation, lying on the surface of the unwrapped wires. Pink-dotted, vertical lines indicate the domain wall width (horizontal scale in nm).

divergent region (shaded red) whose spins point radially inward towards the centre. This is reminiscent of a meron state, where spins point radially inwards/outwards from/to a core. Meron states are topologically equivalent to vortices [22] and have the same exchange energy [23] but a higher magnetostatic energy that would normally preclude their formation in a thin film system. The monopolar, divergent character of such a structure destabilises it in thin films, although effective meron states have been observed in micron-sized anti-ferromagnetically coupled discs [24,25] – a situation where the magnetostatic energy is reduced in comparison to a single disc because the isolated charge produced in one layer is coupled with another of opposing polarity in the second layer. In the present case, the anti-vortex and meron-like states are arranged diametrically across the wire and in this sense are coupled, although their magnetic charges are not balanced.

The benefit of unrolling can also be seen in Fig. 3(b), which now clarifies that the ATDW comprises a vortex/anti-vortex pair, a configuration commonly seen in magnetic thin films and patterned elements as cross-tie DWs [26], although the vortex here shows considerable deviation from circular symmetry. This paired vortex/anti-vortex state was previously predicted as a transient state in tubular structures during DW propagation [11], with the DW mobility showing a dependence on the handedness of the moving wall. Thus, the transition from TDW to ATDW appears more simply as a rotation of spins around the meron-like state of Fig. 3(a) to form the more common vortex state with initially very little change in exchange energy, as shown by the trends in Fig. 2. Finally, the unrolled BPW (Fig. 3(c)) has the simplest surface spin structure. The phase change from either TDW or ATDW to BPW significantly changes their topological spin structures to reduce magnetostatic energy, as shown by Fig. 2.

A useful way of comparing the magnetostatic energy associated with the spin states present on the TDW and ATDW is to consider the modulus of magnetic surface charge $\sigma_s = \boldsymbol{M} . \hat{\boldsymbol{n}}$, where $\hat{\boldsymbol{n}}$ is the unit surface normal and $\boldsymbol{M}$ is the local magnetisation vector. The individual positive and negative contributions to this as a function of DW radius were determined by summing the charge contributions over all nodes and are plotted in Fig. 4. These plots are normalised to $\rho = 2M_sA$, the total charge associated with the magnetisation meeting head-to-head in a wire of cross-sectional area A. Thus, a net charge of (positive) unity means that all of the
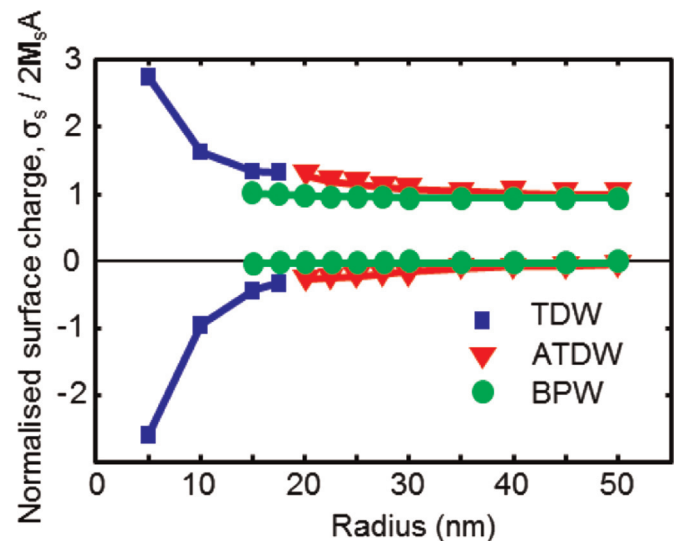
Fig. 4. The variation in surface charge with nanowire radius for the three domain wall types. Charge is calculated by summing over each node on the surface and normalising to the total charge magnitude associated with a head to head domain wall (in a nanowire of cross-sectional area, A), ρ ($=2M_sA$). Both positive and negative contributions are plotted.

internal volume charge arising from the head-to-head nature of the DW has been transported to the surface. It is necessary to consider positive and negative contributions to σ_s instead of the simply the net value because the latter gives a false impression of the magnetostatic energy of a DW. For example, in absolute terms the BPW has the highest net surface charge but, as demonstrated in Fig. 2, the lowest magnetostatic energy.

The BPW plot of Fig. 4 confirms our assertion that the magnetic charge is concentrated at the surface; the normalised σ_s is always close to unity and is exclusively positive. This suggests that the BPW has very little bulk divergence, consistent with its internal curl state. Another interesting feature of Fig. 4 is that it shows a continuous trend from TDW to ATDW with increasing radius, which is intuitive when one considers the facile spin reorientation from a divergent to a curl state. Looking at the internal spin distributions, the cross-sections of Fig. 1 reveal a similarity with the transition between 'flower' and 'C' or 'S' states seen in rectangular 2-D elements or CNTs [27,28]. For narrow 2-D rectangles, the balance between exchange and magnetostatic energies favours a 'flower state', with spins aligned along the rectangle's long axis and only slightly diverging at either end, rather similar to the TDW cross-section in the upper panel of Fig. 1. For wider structures, magnetostatic energy (and surface charge) is reduced at the expense of exchange energy by the formation of a partial flux closure 'C' or 'S' state that is similar to the ATDW cross-section (lower panel of Fig. 1(b)). Overall, the transition lowers the DW symmetry, as shown in Figs. 1 and 3, from a meron-like configuration to a vortex configuration (i.e from achiral to chiral) which comes as a result of the internal twisting of the magnetisation. It is possible that the chiral nature of the ATDW will cause its dynamic behaviour to differ greatly from the TDW, especially in light of results that indicate chiral symmetry breaking in DW propagation [11].

3.2. Cylindrical nanotube results

CNTs are topologically different structures to CNWs, one consequence of which is that magnetisation reversal may occur without the nucleation of singularities [29]. However, studies have shown the DW structures in CNTs to be similar to those in CNWs, particularly at small radii, where the TDW still forms [12]. An important difference is that the BPW does not exist, since there is no material along the tube axis to support a spin singularity. Instead, a vortex DW (VDW, not shown) forms and has a similar external spin structure to the BPW. Fig. 5 summarises the results of simulations of CNT structures for tubes of two internal diameters and shows the VDW to exist across the range of simulated geometries. Neither of the other two DW types formed so readily and the existence of metastable states is harder to determine, presumably because any energy barrier between metastable and ground states is too small.

An ATDW was found to be metastable for the single case of a CNT with an inner radius of 5 nm and an outer radius of 20 nm, the unrolled external and internal surfaces of which are illustrated in Fig. 6. The unrolled view shows the ATDW to be intermediate in character, with a similar anti-vortex region (in blue) to that seen in the CNW of Fig. 3(a) and (b) but with a distorted divergent state (shaded red) that has aspects of both the meron-like state of Fig. 3 (a) and the vortex of Fig. 3(b). This state could not be stabilised in simulations using other radii, irrespective of how the simulation's starting state was constructed, although it has been predicted as a transient state at greater radii than considered here [11]. The apparent stability can be explained by considering that when moving from CNWs to CNTs, the low divergence bulk is replaced by extra surface charge on the internal surface. Fig. 5 also shows that the TDW becomes less stable with increasing inner radius; as we move from an inner radius of 5–10 nm the TDW is no longer the ground
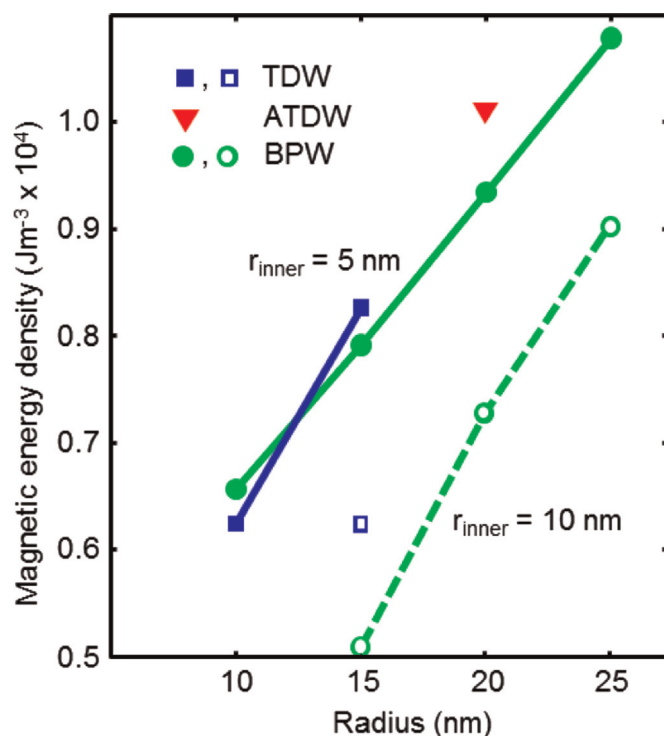

Fig. 5. The magnetic energy density of cylindrical permalloy nanotubes with an internal bore radius of (full lines, full markers) 5 nm and (dashed line, hollow markers) 10 nm. The only stable ATDW simulation and 10 nm TDW simulation are indicated as single points.
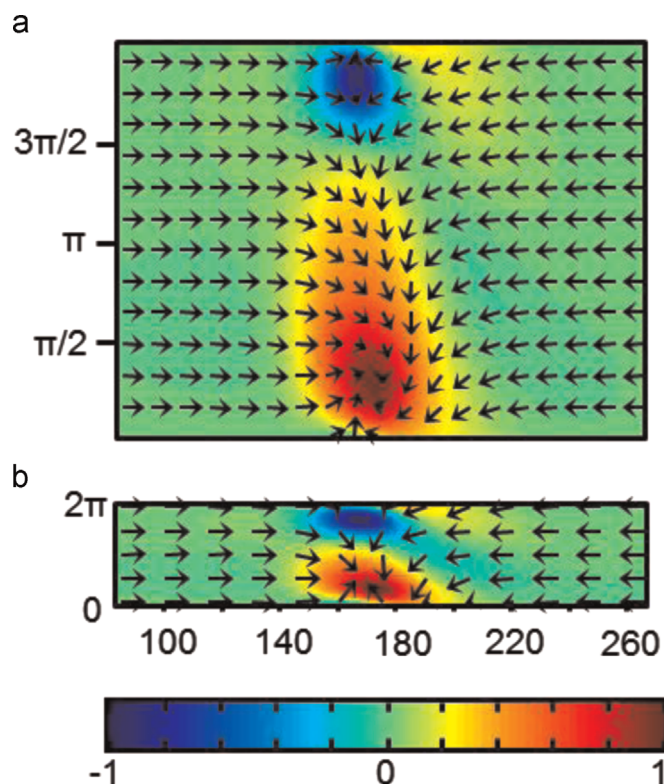

Fig. 6. The unrolled magnetisation of a ATDW within a cylindrical permalloy nanotube, showing the variation across the (a) exterior and (b) interior surfaces. The colour scheme and figure orientation are as Fig. 3.

state, presumably because the extra surface charge on the inner surface destabilises the TDW. Despite the fact that the CNTs simulated here have smaller inner and outer radii, we cannot rule

out the possibility of transient ATDWs [11]. It may be the case that transient states are more likely to form in the CNTs simulated here given that they can be stabilised as a static state for one particular inner/outer radius combination. This raises the possibility that Walker breakdown may occur more readily here than for the thinner CNTs that were reported previously.

4. Summary

In summary, we have constructed a phase diagram of ground and metastable magnetic states in cylindrical nanowires and nanotubes of varying radius. Our phase diagram confirms that the TDW is the ground state for thin nanowires but at larger radii (20 nm in the case of permalloy) a ground state BPW is favoured. However, a metastable ATDW is shown to exist with only a slightly higher energy. This may have implications for dynamic systems and the range of geometries that support Walker breakdown by the nucleation of vortex/anti-vortex pairs. The metastable ATDW is seen to have similarities to the structure of the TDW, albeit with lower symmetry and a more rotational character. The transition from TDW to ATDW occurs due to lowering the surface charge at a cost of increased exchange energy. These simulations provide insight into symmetry breaking of DWs in CNWs and CNTs and, as well as aiding the interpretation of experimental investigations, can be used as the basis for future studies on DW dynamics.

Acknowledgements

References

[1] S.S.P. Parkin, M. Hayashi, L. Thomas, Magnetic domain-wall racetrack memory, Science 320 (2008) 190.
[2] M. Hayashi, L. Thomas, R. Moriya, C. Rettner, S.S.P. Parkin, Current-controlled magnetic domain-wall nanowire shift register, Science 320 (2008) 209.
[3] D.A. Allwood, G. Xiong, C.C. Falkner, D. Atkinson, D. Petit, R.P. Cowburn, Magnetic domain-wall logic, Science 309 (2005) 1688.
[4] Y. Nakatani, A. Thiaville, Domain wall dynamics in nanowires and nanostrips, Spin Dynamics in Confined Magnetic Structures III (Top. Appl. Phys. vol. 101), 2006.
[5] Y. Nakatani, A. Thiaville, J. Miltat, Head-to-head domain walls in soft nano-strips: a refined phase diagram, J. Magn. Magn. Mater. 290 (2005) 750.
[6] L. Bogart, D. Atkinson, K. O'Shea, D. McGrouther, S. McVitie, Dependence of domain wall pinning potential landscapes on domain wall chirality and pinning site geometry in planar nanowires, Phys. Rev. B 79 (2009) 054414.

[7] N.L. Schryer, L.R. Walker, The motion of 180° domain walls in uniform dc magnetic fields, J. Appl. Phys. 45 (1974) 5406.
[8] Y. Nakatani, A. Thiaville, J. Miltat, Faster magnetic walls in rough wires, Nat. Mater. 2 (2003) 521.
[9] M. Yan, A. Kákay, S. Gliga, R. Hertel, Beating the Walker limit with massless domain walls in cylindrical nanowires, Phys. Rev. Lett. 104 (2010) 057201.
[10] M. Yan, C. Andreas, A. Kákay, F. García-Sánchez, R. Hertel, Fast domain wall dynamics in magnetic nanotubes: suppression of Walker breakdown and Cherenkov-like spin wave emission, Appl. Phys. Lett. 99 (2011) 122505.
[11] M. Yan, C. Andreas, A. Kákay, F. García-Sánchez, R. Hertel, Chiral symmetry breaking and pair-creation mediated Walker breakdown in magnetic nano-tubes, Appl. Phys. Lett 100 (2012) 252401.
[12] P. Landeros, S. Allende, J. Escrig, E. Salcedo, D. Altbir, Reversal modes in magnetic nanotubes, Appl. Phys. Lett. 90 (2007) 102501.
[13] R. Hertel, Computational micromagnetism of magnetisation processes in nickel nanowires, J. Magn. Magn. Mater. 249 (2002) 251.
[14] N. Biziere, C. Gatel, R. Lassalle-Balier, M.C. Clochard, J.E. Wegrowe, E. Snoeck, Imaging the fine structure of a magnetic domain wall in a Ni nanocylinder, Nano Lett. 13 (2013) 2053.
[15] T. Fischbacher, M. Franchin, G. Bordignon, H. Fangohr, A systematic approach to multiphysics extensions of finite-element-based micromagnetic simula-tions: Nmag, IEEE Trans. Magn. 43 (2007) 2896.
[16] M.J. Donahue, Micromagnetic investigation of periodic cross-tie/vortex wall geometry, Adv. Condens. Matter Phys. 2012 (2012) 1.
[17] C. Brownlie, S. McVitie, J.N. Chapman, C.D.W. Wilkinson, Lorentz microscopy studies of domain wall trap structures, J. Appl. Phys. 100 (2006) 033902.
[18] W. Zhang, R. Singh, N. Bray-Ali, S. Haas, Scaling analysis and application: phase diagram of magnetic nanorings and elliptical nanoparticles, Phys. Rev. B 77 (2008) 144428.
[19] P. Landeros, J. Escrig, D. Altbir, D. Laroze, P. d'Albuquerque e Castro, Scaling relations for magnetic nanoparticles, Phys. Rev. B 71 (2011) 094435.
[20] J.A. Otálora, J.A. López-López, P. Landeros, P. Vargas, A.S. Núñez, Breaking of chiral symmetry in vortex domain wall propagation in ferromagnetic nano-tubes, J. Magn. Magn. Mater. 341 (2013) 86.
[21] A. Thiaville, J.M. García, J. Miltat, Domain wall dynamics in nanowires, J. Magn. Magn. Mater. 242–245 (2002) 1061.
[22] N.D. Mermin, The topological theory of defects in ordered media, Rev. Mod. Phys. 51 (1979) 591.
[23] M. Yan, H. Wang, C.E. Campbell, Unconventional magnetic vortex structures observed in micromagnetic simulations, J. Magn. Magn. Mater. 320 (2008) 1937.
[24] C. Phatak, A.K. Petford-Long, O. Heinonen, Direct observation of unconven-tional topological spin structure in coupled magnetic discs, Phys. Rev. Lett. 108 (2012) 067205.
[25] S. Wintz, C. Bunce, A. Neudert, M. Korner, T. Strache, M. Buhl, A. Erbe, S. Gemming, J. Rabbe, C. Quitmann, J. Fassbender, Topology and origin of ef-fective spin meron pairs in ferromagnetic multilayer elements, Phys. Rev. Lett. 110 (2013) 177201.
[26] N. Wiese, S. McVitie, J.N. Chapman, A. Capella-Kort, F. Otto, On the scaling behaviour of cross-tie domain wall structures in patterned NiFe elements, Europhys. Lett. 80 (2007) 57003.
[27] X. Liu, J.N. Chapman, S. McVitie, C.D.W. Wilkinson, Reversal mechanisms and metastable states in magnetic nanoelements, J. Appl. Phys. 96 (2004) 5173.
[28] P. Landeros, O. Suarez, A. Cuchillo, P. Vargas, Equilibrium states and vortex domain wall nucleation in ferromagnetic nanotubes, Phys. Rev. B 79 (2009) 024404.
[29] A.S. Arrott, B. Heinrich, A. Aharoni, Point singularities and magnetisation re-versal in ideally soft ferromagnetic cylinders, IEEE Trans. Magn. 15 (1979) 1228.